# Bottom Stress Estimates from Vertical Dissipation Rate Profiles on the Continental Shelf

RICHARD K. DEWEY

*College of Oceanography, Oregon State University, Corvallis, Oregon*

WILLIAM R. CRAWFORD

*Institute of Ocean Sciences, Department of Fisheries and Oceans, Sidney, British Columbia, Canada*

(Manuscript received 3 February 1987, in final form 25 February 1988)

ABSTRACT

Measurements of the near-bottom distribution of the turbulent dissipation rate on the continental shelf west of Vancouver Island are used to calculate bottom stress. A free-falling vertical profiler with microstructure shear probes was used to measure the dissipation rate, from near the surface to within 0.15 m of the bottom. The shear probes measure velocity gradients at scales within the viscous subrange of the turbulence and therefore directly measure the rate at which kinetic energy is dissipated by viscosity. Friction velocities are computed from the formula $u_* = (\epsilon \kappa z/\rho)^{1/3}$, where the dissipation rate $\epsilon$ is measured in the constant stress layer. The technique is more reliable than estimates of the dissipation rate obtained by fitting spectral slopes to velocity spectra at scales in the inertial subrange. Near-bottom current measurements indicate that the bottom stress values obtained from the turbulent measurements are well correlated with the current magnitude. An estimate of the drag coefficient indicates that the bottom is hydrodynamically smooth and that bottom stress estimates from current data alone would overestimate the stress by four times, possibly due to the influence of form drag.

## 1. Introduction

The structure of the bottom boundary layer in coastal seas has been of interest to oceanographers for many years, and it is only recently that the instrumentation and technology required to sample the important physical properties have been available. The importance of bottom parameters, such as the bottom stress and the bottom roughness, on the dynamics governing the velocity structure within the boundary layer is well recognized (e.g., Richards 1982; Soulsby 1983; Grant et al. 1984; Grant and Madsen 1986). The continental shelf provides an excellent observation area for bottom boundary layer studies. The currents are predominantly tidal and wind driven, and the water depth (<200 m) provides an easily accessible boundary layer.

In June 1985 a boundary layer experiment was carried out on the continental shelf west of Vancouver Island (Fig. 1a). Results presented here are from a portion of this survey and show how turbulent microstructure measurements made with shear probes can be used to estimate the bottom stress. The technique is potentially more accurate than bottom stress estimates made from velocity measurements at scales within the inertial subrange or from current measurements made outside the constant stress layer and fitted to logarithmic functions. Some data are also presented from Hecate Strait in northern British Columbia (Fig. 1b), obtained in 1983.

The following section describes the basic theories for obtaining bottom stress estimates from measurable quantities. The shortcomings of some of these techniques are indicated. Next, the details of the boundary layer experiment and the method of calculating the dissipation rate are described in sections 3 and 4. Section 5 is a discussion of the considerations in obtaining reliable dissipation rate and bottom stress estimates within bottom boundary layers. Dissipation rate profiles and bottom stress estimates are presented in section 6. Section 7 is a discussion on the results.

Before we proceed it may be useful to establish what is meant by the terms homogeneity and stationarity. Both terms will be used here in the discussion of turbulence measurements in the ocean. Homogeneity implies uniform conditions in space, unchanged by a translation. Stationarity refers to changes in time. Under certain conditions a flow can be either or both homogeneous and stationary, when small space and time scales are considered. Conversely, real flows are always inhomogeneous and nonstationary when large distances and times are considered. At certain stages of the analysis either or both homogeneity and stationarity will be assumed, and attempts to justify these assumptions will be made. The terminology is further complicated by the fact that Taylor's *frozen turbulence* hypothesis has been invoked to get vertical shear ($\partial u/\partial z$) from the differentiated shear probe voltage (Dewey et

*Corresponding author address:* Dr. Richard K. Dewey, College of Oceanography, Oregon State University, Corvallis, Oregon 97331.

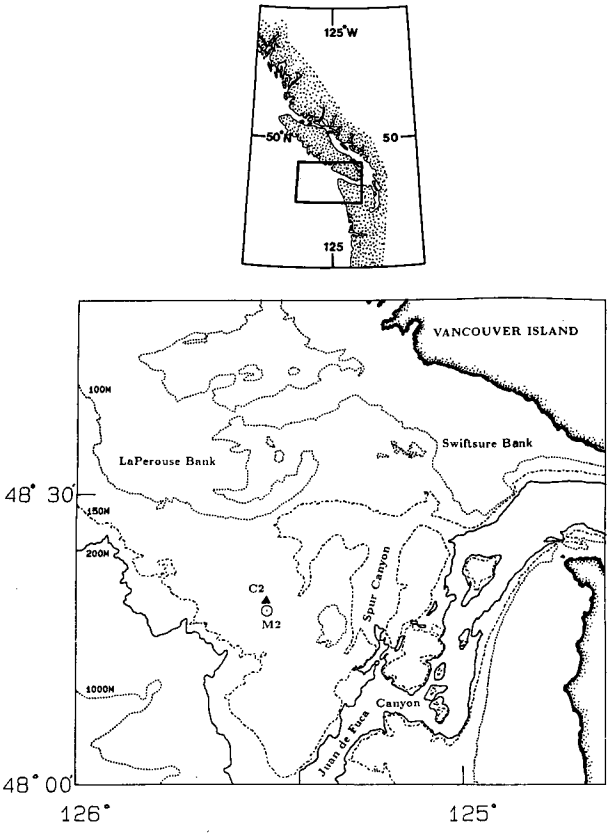


FIG. 1a. The continental shelf region west of Vancouver Island. Microstructure data were collected at M2 in June 1985. A current mooring at C2 had meters at 3, 5, 10, 30 and 95 m above the bottom. The total depth near M2 is 135 m.

al. 1987). This transforms time variations into space variations, and considerations of stationarity into conditions of homogeneity and visa-versa. In other words, the problems of nonstationarity in time-series analysis become problems of inhomogeneity in space-series analysis.

## 2. Bottom stress estimates: Theory

An estimate of the bottom stress may be derived from: 1) the time-averaged velocity profile near the bottom, 2) direct measurements of the Reynolds stress $-\rho\overline{u'w'}$, and 3) the turbulent dissipation rate measured within the constant stress layer. All three techniques have physical limitations. In the following discussion the shear stress at the bottom will be denoted by $\tau_0$ and the roughness of the bottom surface will be characterized by $z_0$. The importance and influence of wave-induced stresses are acknowledged, but in the following discussion it will be assumed that current shear alone dominates. This is valid in deeper regions where surface wave motion does not penetrate to the bottom, except perhaps during storms. For more details on the influence of waves and swell in the bottom boundary layer the reader is referred to Grant and Madsen (1979).

### a. *Velocity profile technique*

The mean velocity distribution in the boundary layer is a function of the bottom shear stress $\tau_0$, the roughness parameter $z_0$, the distance to the bottom $z$, and the fluid properties $\rho$ and $\mu$, where $\rho$ is the seawater density and $\mu$ is the dynamic viscosity. The characteristic velocity scale in the bottom boundary layer is called the friction velocity, $u_* \equiv \sqrt{\tau_0/\rho}$.

It has been observed that the Reynolds stress near the bottom is constant over a layer, denoted the constant stress layer (CSL), and is equal to the bottom stress $\tau_0$. With a linear mixing length $l = \kappa z$ the mean shear $\partial\bar{U}/\partial z$ in the constant stress layer is given by the "law of the wall",

$$\frac{\partial \bar{U}}{\partial z} = \frac{u_*}{\kappa z}, \tag{1}$$

where $\kappa$ is the von Kármán constant ($\sim$0.41). Upon integration we obtain the logarithmic velocity profile,

$$\bar{U} = \frac{u_*}{\kappa} \ln \frac{z}{z_0}, \tag{2}$$

where $z_0$ is the constant of integration and represents

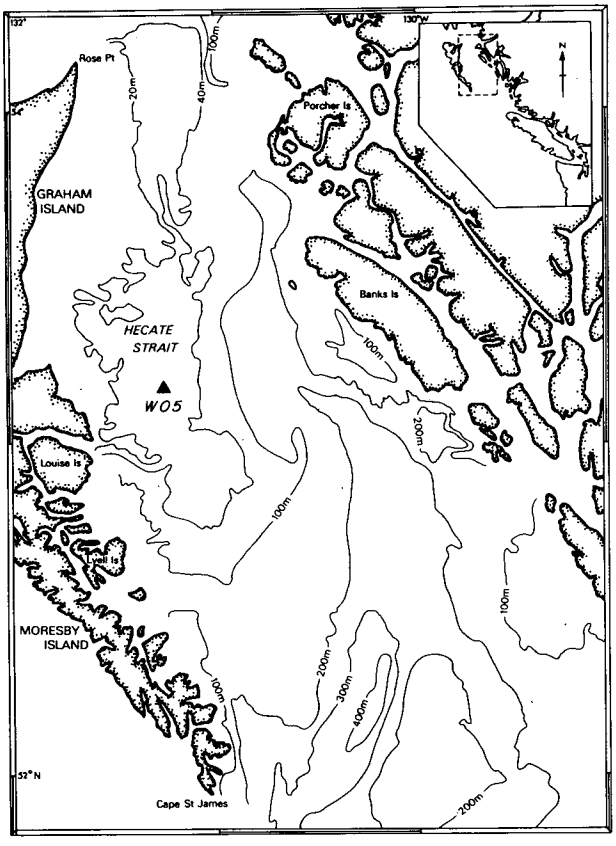


FIG. 1b. Hecate Strait region east of the Queen Charlotte Islands. Microstructure profiles were collected at station W05 in July 1983. The depth near W05 is 35 m.

a length scale proportional to the roughness elements at the bottom. A similar profile is obtained for a turbulent flow over a hydrodynamically smooth bottom, where the surface elements do not protrude through the viscous sublayer. Under such conditions $z_0$ in (2) is replaced by a viscous length scale proportional to the height, $\delta$, of the viscous sublayer and the constant of integration is chosen to match the velocity at the top of the viscous sublayer ($\delta u_*^2/\nu$),

$$\bar{U} = \frac{u_*}{\kappa} \ln \frac{z}{\delta} + \frac{\delta u_*^2}{\nu}. \tag{3}$$

By measuring the mean velocity at a number of heights above the bottom, one can do a linear least-squares fit between $\bar{U}$ and $\ln z$ in (2), from which $u_*$ and $z_0$ can be calculated from the slope and intercept, respectively. The roughness parameter $z_0$ can also be estimated from the bottom microtopography, but it is not clear how this calculation can be successfully repeated from one environment to another (Grant and Madsen 1986).

Grant et al. (1984) measure the velocity at heights of 28, 53, 103, and 203 cm above the bottom and find that in order to maintain uncertainties in $u_*$ of less than ±25%, they require linear regression coefficients from their least squares fit to (2) of better than $R^2 = 0.993$. Extremely accurate and stable current measurements are required to obtain only adequate estimates in $u_*$, because the logarithmic velocity profile predicts small shears at the operating heights of current meters, while simultaneously predicting large shears as $z$ approaches $z_0$, where current meters work less well (Gust 1985). Accurate measurements of the mean current ($\bar{U}$) close to the bottom (<1 m) are difficult due to the large ratio of fluctuating turbulent velocities to the mean flow, the influence of form drag on the current (Chriss and Caldwell 1982), and the low overall speeds which are often near the stall speed and resolution of the current meter (Gust 1985). Current measurements at larger distances from the bottom ($z > 1$ m) are more stable but may be outside the CSL and not representative of the dynamics governed by the bottom friction.

### b. *Reynolds stress estimates*

The most direct, yet most difficult method of estimating the bottom stress $\tau_0$ is to assume a layer of constant Reynolds stress near the bottom,

$$\tau_0 = -\rho\overline{u'w'} = \text{const}, \tag{4}$$

and measure $u'$ and $w'$ in this layer. Soulsby (1983) measures $u'$ and $w'$ at fixed heights above the bottom using electromagnetic current meters. The product $\overline{u'w'}$ is calculated over 8 to 12 minute time series. These measurements are restricted to longer wavelengths and are very sensitive to the orientation and tilting of the instrumentation ($\tau_0$ varies ±10% per degree of tilt; Soulsby 1983). Also, in order to recover the full covariance $\overline{u'w'}$, theoretical spectral shapes are used to extrapolate the measured spectra to higher wavenumbers, within the inertial subrange.

### c. *Dissipation rate technique*

Within the well-mixed portion of a slowly accelerating bottom boundary layer (<10 m) there is a local balance between the rate of production of turbulent kinetic energy through the Reynolds stress working on the mean share and the rate of viscous dissipation of that energy,

$$-\rho\overline{u'w'}\frac{\partial \bar{U}}{\partial z} = \epsilon, \tag{5}$$

where $\epsilon$ is the dissipation rate of turbulent kinetic energy per unit volume (hence the factor of $\rho$ in the formula). Within the constant stress layer (CSL) the Reynolds stress is equal to the bottom stress and is given by (4), and with the mean shear given by (1), it follows that

$$\epsilon = \rho \frac{u_*^3}{\kappa z}. \tag{6}$$

If $\epsilon$ can be measured within the CSL, at a distance $z$ from the bottom, then $u_*$ can be calculated. The cubic dependence means that errors in $\epsilon$ translate to smaller errors in $u_*$, and intermittency in $\epsilon$ results in smaller fluctuations in $u_*$ and $\tau_0$.

#### 1) Inertial dissipation rate technique

Previous estimates of the dissipation rate $\epsilon$, for bottom stress analysis (Grant et al. 1984; Gross and Nowell 1985; Huntley and Hazen 1988) have been calculated from measurements of turbulent velocities at inertial scales, and will be denoted as the *inertial* dissipation technique. This calculation follows from the theories of Kolmogoroff (1941). The theory requires that the local Reynolds number be sufficiently high so that an inertial subrange exists between the larger energy-containing scales and the smaller viscous dissipation scales.

The turbulent velocity spectrum within the inertial subrange then takes on the simple form,

$$E(k) = A\left(\frac{\epsilon}{\rho}\right)^{2/3} k^{-5/3}, \tag{7}$$

where $A$ is the three dimensional Kolmogoroff constant ($A \approx 1.589$, Nasmyth 1986, personal communication), and $k$ is the local three-dimensional wavenumber. The three dimensional velocity spectrum $E(k)$ is rarely measured directly, but can be obtained from spectra of single velocity components by assuming isotropy (Monin and Yaglom 1975). If the Reynolds number is sufficiently large and an inertial subrange

exists, then the friction velocity can be found from (6) and (7),

$$u_* = \left\{\frac{E(k)k^{5/3}}{A}\right\}^{1/2}(\kappa z)^{1/3}, \quad (8)$$

where $k$ is taken within the inertial subrange only.

Although this theory is rather straightforward, the existence of an inertial subrange in benthic turbulence can not always be assumed. Huntley (1988) finds that, in most benthic constant stress layers, the assumptions in Kolmogoroff's theory are not satisfied, in that there is no separation of the production–dissipation scales. He concludes that $u_*$ estimates calculated from velocity measurements within the inertial subrange are valid for flows only if $u_* > 0.8 \pm 0.2$ cm s$^{-1}$, or when measurements are made at heights where there is no separation of the production and dissipation scales. In the later case, corrections must be applied to the spectra that extrapolate the inertial subrange theories to wavenumbers outside the inertial subrange. Gross and Nowell (1985) calculate the friction velocity from velocity measurements at inertial scales and find that they required $u_* > 2.0$ cm s$^{-1}$ in order to resolve the full dissipation rate within 1 meter of the bottom. However, most of their estimates are therefore calculated from dissipation rate values obtained above $z = 1$ m where an inertial subrange is more likely to exist but where a constant stress layer may not.

The assumptions of homogeneity [required for (5)] and isotropy [required for (7)] are valid for different scales of the velocity fluctuations, at different heights $z$ from the boundary. To a first-order approximation, turbulence is isotropic at wavenumbers $k > 2\pi/z$ (Pond 1965). The constant stress layer, as suggested by laboratory measurements (Hinze 1975), could be restricted to heights $z < \mu 2000/\rho u_*$; so, as the Reynolds number and $u_*$ increase and the inertial subrange develops, the height of the constant stress layer simultaneously decreases, with the result that an isotropic inertial subrange may never exist within the constant stress layer.

### 2) Viscous dissipation rate technique

The dissipation technique is not limited by the factors noted above if the dissipation rate $\epsilon$ is calculated from velocity measurements at higher wavenumbers, within the viscous subrange. Successful measurements of the dissipation rate of oceanic turbulence have been obtained using shear probes as described by Osborn (1974), Crawford and Osborn (1979), Osborn and Crawford (1980), and Oakey and Elliott (1982). Shear probes mounted on profiling vehicles are used to measure velocity fluctuations at wavelengths between ~0.01 and ~1.0 m, a band which usually spans the viscous subrange. This subrange is the band of scales (wavelengths) where the kinetic energy is actually being dissipated directly by viscous forces. Therefore, velocity measurements at scales within the viscous subrange (dissipation scales) may be used to estimate direct contributions to the total dissipation rate $\epsilon$, *without the need to fit the data to particular spectral shapes.* The component of turbulent shear ($\partial u/\partial z$) is almost fully measured by a shear probe (Dewey 1987), and the assumption of isotropy is used only to approximate the remaining contributions to $\epsilon$, such as $\partial u/\partial x$ and $\partial w/\partial z$ (Monin and Yaglom 1975). The universal spectrum of Nasmyth (1986, personal communications) is used to estimate the small portion of the $\partial u/\partial z$ signal outside the measured bandwidth. This $\epsilon$ is then used in (6) to estimate the friction velocity and therefore the bottom stress. This is the dissipation technique, distinct from the *inertial* dissipation technique of Grant et al. (1984) and Gross and Nowell (1985).

## 3. Experimental details

Data presented here were obtained during two cruises, one in July 1983 to Hecate Strait and the other to the continental shelf west of Vancouver Island in June 1985 (Fig. 1). The Hecate Strait data were obtained in water 35 m deep at W05 (53°11′N, 131°14′W) during very light winds and calm seas. The currents in Hecate Strait are composed of a dominant semidiurnal tide and a weaker wind-driven circulation. Data from west of Vancouver Island were collected at station M2 (48°18.5′N, 125°30.25′W) in 135 m of water. In both cases, surface wave heights were too small to influence the bottom boundary layer. A current-meter mooring at C2 located 1 km north of M2 had Aanderaa current meters located at heights of 3, 10 and 30 m above the bottom, a fast sampling Geodyne meter at 5 m above the bottom and an InterOcean S4 current meter at 40 m below the surface (~95 m from the bottom). The meters sampled at intervals ranging from 1 second to 5 minutes. The near-bottom flow at C2 (in June) is primarily composed of a diurnal and semidiurnal tide (~80%) and a mean, southerly current (~20%). The diurnal current is of tidal origin, due to anomalously strong diurnal-period shelfwaves in this region (Crawford and Thomson 1984; Crawford 1984).

The microstructure profiler FLY II is described by Dewey et al. (1987). The profiler is a tethered instrument that is released from the surface and is permitted to land on the bottom. A probe guard extends in front of the shear and temperature probes located at the lower end of the profiler and has been designed to protect the probes when the profiler hits the bottom, without unduly increasing instrument vibrations that would contaminate the shear probe signal during descent. The fall speed was ~0.65 m s$^{-1}$. The shear, temperature, conductivity, pressure, and two tilt signals are digitized, transmitted to the ship, displayed and stored for later analysis.

The sampling procedure employed on the shelf west of Vancouver Island consisted of a CTD profile with a near-bottom oxygen sample followed by a set of ten consecutive microstructure profiles. The entire series was repeated every two hours. The ten microstructure profiles consisted of one surface-to-bottom profile followed by three groups of three profiles, one complete profile (~130 m) and two through the bottom 40 m. This procedure provided three groups of three quasi-synoptic profiles through the bottom boundary layer. The elapsed time for each group was approximately 10 minutes. The elapsed time for a complete series of 10 profiles was nearly 40 minutes. In Hecate Strait, where the total water depth was only ~35 m, series of 10 and 20 full profiles were obtained every hour. A total of 110 profiles were obtained at M2 and 210 at W05 in Hecate Strait.

## 4. Dissipation rate calculation

The dissipation rate per unit volume $\epsilon$ is calculated from the variance of the shear time series (Osborn 1974),

$$\epsilon = 7.5\mu\overline{\left(\frac{\partial u}{\partial z}\right)^2}. \tag{9}$$

The variance is estimated from the power spectrum of the shear signal. This method was first introduced for shear probe measurements by Osborn (1974). Spectral techniques are used so that noise in the signal can be isolated, and the spatial response of the shear probe and high and low frequency attenuation in the electronics can be compensated for.

The microstructure shear is obtained from the differentiated shear probe signal $V_0$, which is proportional to $\partial u/\partial t$, using Taylor's hypothesis,

$$\frac{\partial u}{\partial z} = \frac{1}{W}\frac{\partial u}{\partial t} = \frac{V_0}{G2\sqrt{2}SW^2}, \tag{10}$$

where $W$ is the fall speed, $G$ is the differentiator gain, $S$ is the shear probe calibration, $2\sqrt{2}$ a calibration constant and $V_0$ the differentiated output voltage. Once the shear $\partial u/\partial z$ time series is obtained, it is subdivided into overlapping sections from which power spectra are calculated.

Before the shear data are cosine-tapered and passed to the Fourier transform, the mean and linear trend in the data are removed. Removing the trend reduces the leakage of low frequency energy to dissipation scales.

The power spectrum of $\partial u/\partial z$ is the one dimensional dissipation spectrum $k_3{}^2\phi_{11}(k_3)$. By assuming isotropy we have (Monin and Yaglom 1975),

$$\epsilon = 7.5\mu\int_0^\infty k_3{}^2\phi_{11}(k_3)dk_3. \tag{11}$$

The integration limits actually used in the variance calculation, $k_l$ and $k_u$, are selected to minimize the contributions to the integral from regions of the spectrum, both at low ($k < k_l$) and high ($k > k_u$) wavenumbers, that are contaminated by noise. The contributions lost by selecting a band narrower than 0 to $\infty$ are estimated and added to (11) (Dewey 1987). The variance added is typically <15% for dissipation rates $\epsilon > 10^{-5}$ W m$^{-3}$.

## 5. Accuracy in $\epsilon$ and $u_*$ calculations

Although the following discussion pertains directly to shear probe measurements, the considerations are applicable for most techniques of estimating $\epsilon$. The accuracy in a calculation of $\epsilon$ within the bottom boundary layer depends on six factors. Four of these (1–4) are similar to those discussed by Soulsby (1980) for $\overline{u'w'}$ measurements, the fifth addresses the assumption of isotropy, and the sixth looks at the uncertainties associated with the various calibrations necessary in estimating the dissipation rate from shear probe measurements. These factors are as follows.

1) *The loss of low- and high-frequency information due to the length of the time series analyzed and the digitization rate, respectively:* If the time series, of say $J$ points, is too short then low-frequency information will be lost. Near the ocean bottom this loss must be balanced with the requirements of homogeneity. If the digitization rate is too low, or the response of the probe too slow, significant high-frequency contributions will not be resolved.

The first consideration is to prove that the records selected are long enough to resolve the low-frequency portion of the dissipation spectrum. Dewey (1987) shows that a minimum percentage (e.g., 5%) of the universal spectrum is lost when the minimum wavenumber recovered $k_l$ is

$$k_l = k_{5\%} \approx 0.04k_s, \tag{12}$$

where $k_s = (\epsilon\rho^2/\mu^3)^{1/4}$ is the Kolmogoroff wavenumber. The number of points in the time series section required to recover the spectrum down to $k_{5\%}$ is then given by

$$J_{5\%} = \frac{2\pi}{Wk_{5\%}\Delta t} = \frac{2\pi}{W(0.04)k_s\Delta t}, \tag{13}$$

where $\Delta t$ is the digitization rate. If $J$, the number of points contributing to the power spectrum, is larger than this lower limit $J_{5\%}$, then less than 5% of the spectrum will be lost. If, for example we choose $\epsilon = 5.0 \times 10^{-4}$ W m$^{-3}$ and $\mu = 1.54 \times 10^{-3}$ kg (m s)$^{-1}$, then $k_s = 616$ m$^{-1}$, and if $\Delta t = 3.646 \times 10^{-3}$ s and $W \approx 0.63$ m s$^{-1}$ as is the case with the present profiler, then $J_{5\%} = 111$ points. This minimum time series length increases slowly with decreasing $\epsilon$, as $J_{5\%} \propto \epsilon^{-1/4}$. The

minimum number of points used in this paper is $J = 128$. The actual percentage lost by choosing $k_l > 0$ has been calculated for each $\epsilon$ value assuming a universal spectrum and added to the integrated estimate.

We can also estimate the friction velocity associated with the flow when the lowest wavenumber recovered is $k_{5\%}$. For a time series of 128 points, the lowest wavenumber resolved is $k_L = (2\pi/0.3) \approx 20.9\ \text{m}^{-1}$. For the first time series section starting at 0.15 m above the bottom, we find that after substituting for (6) and (12), $k_{5\%}$ is resolved when $u_* > 0.24\ \text{cm s}^{-1}$. When $u_* < 0.24\ \text{cm s}^{-1}$ more that 5% of the variance is not resolved by a 128 point spectrum. The percentage lost, whether less than or greater than 5%, is estimated (Dewey 1987) and added to the recoverable variance.

The digitization rate of the present system has an associated Nyquist wavenumber of $k_N \approx 2.1\ \text{cm}^{-1}$. The probe can only resolve to a wavenumber of approximately $k \approx 1.7\ \text{cm}^{-1}$, so the sampling rate is limited by the response of the probe, and not the digitization rate.

2) *Stationarity and homogeneity:* Spectral time series analysis assumes that the section of time series is stationary, in that the variance does not change from the start of the record to the end. Homogeneity is required for (5) and (6) to hold.

The shear time series used to calculate the dissipation rate is a vertical "space series", and inhomogeneity in the vertical distribution of the turbulence will result in a nonstationary time series. If (6) is the distribution of $\epsilon$ in the constant stress layer, then the time series of $\partial u/\partial z$ is nonstationary. To reduce (but not eliminate) the effects of this nonstationarity, the vertical resolution in $\epsilon$ was enhanced by choosing short time series sections for small $z$. The first three sections above the bottom have $J = 128$ points. The sections are overlapped in most cases by 50%, and increase in length as $z$ increases (i.e., $J = 128, \cdots, 256, \cdots, 512, \cdots, 1024, \cdots$), as follows,

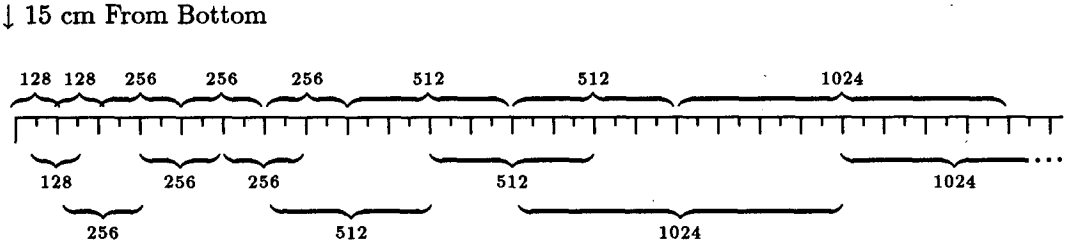


Overlapping the time series reduces the number of independent observations but is one of the most efficient ways of sectioning, with minimal information loss after cosine windowing (Press et al. 1986). The shorter sections near the bottom improve the vertical resolution and the problems of nonstationarity, but with lower confidence in the individual $\epsilon$ values.

A more specific nonstationary character of the flow within the constant stress layer is implied by the distribution (6) for the dissipation rate (or variance $\overline{(\partial u/\partial z)^2}$) which suggests an increase of 60% between the bottom and top of the section nearest to the sea floor. Thus a slight error (overestimate) is introduced in $u_*$ by assuming that the time series in the constant stress layer is homogeneous (stationary) and that the recovered variance $\overline{(\partial u/\partial z)^2}$ represents the value at the center of the time series $\bar{z}$. If (6) is the true distribution of $\epsilon$ within the constant stress layer, then the variance calculated by (11) is proportional to the dissipation rate at a slightly lower height than the centre of the time series section. The maximum error in $\bar{z}$ introduced by this assumption is 9% for the first 128 point time series, which represents a 3% error in $u_*$. This error in $u_*$ is reduced by $\frac{2}{5}$ for each subsequent estimate up from the ocean bottom.

Because we compute spectra only to separate signal from noise (Dewey, 1987), without curve fitting, nonstationarity in $\overline{(\partial u/\partial z)^2}$ interferes little with our method of computing the bottom stress. We could instead take the raw $\partial u/\partial z$ signal, square it and fit it to a $z^{-1}$ distribution [using (6) and (9)], thereby determining the same $\epsilon$ and $u_*$ values, but with reduced confidence. The spectral shape may be distorted slightly due to the nonstationary, and universal forms may not be exhibited, but our variance estimation is only weakly dependent on spectral shape.

FLY II penetrates the bottom 5 m in less than 8 s, a period much shorter than any fluctuation in the large scale features of the flow (such as the tides, or internal waves). The series of ten profiles taken to improve the confidence in the calculated $u_*$ values required 40 minutes, during which time the large scale flow (tide) is stationary (Dewey 1987), but the effects due to internal waves are not.

3) *Sampling variability:* The random error associated with making single estimates in a stochastic field can be reduced by increasing the number of estimates in an ensemble average, but with too many samples

the series tends to be too long in time to satisfy stationarity.

Sample variability arises when single estimates of an intermittent or stochastic process are obtained. Single profiles of $\epsilon$ can be thought of as synoptic. Consecutive profiles, it turns out give surprisingly similar estimates of $u_*$, with maximum variations of order $\approx$30%. More typically, the variations are less than 15%. This is likely due to the fact that measurements at viscous scales are more likely to be isotropic than measurements at larger scales (Scorer 1985). Averaging consecutive $\epsilon$ profiles reduces the effects of intermittency, with standard deviations in the average dissipation rate estimates in the order $\sim$15%, and standard deviations in $u_*$ of less than 10%.

Turbulent dissipation rate and bottom stress distributions are lognormal and the proper indicator of the degree of intermittency is the "intermittency factor" $\sigma^2_{\ln X}$ described by Baker and Gibson (1987). This parameter is the variance of the natural logarithm of the stationary variable ($X$). The intermittency factor $\sigma^2_{\ln u_*}$ is computed over each one-hour observation period, with an average value $\overline{\sigma^2_{\ln u_*}} = 0.11$ ($\pm$0.05) (where the uncertainty is one standard deviation calculated from the eleven lognormal variances). This represents an average intermittency factor for the bottom stress estimates of $\sigma^2_{\ln \tau_0} = 0.22$. The estimated intermittency factors indicate that sufficient sampling of the intermittent turbulent velocities has been made and that the estimated bottom stresses are representative of the true stress (Baker and Gibson 1987).

4) *Sensor response:* The sensor used to measure the turbulent fluctuations will likely have spatial and temporal response limitations. The small-scale spatial response is usually determined by the size of the sensor and the range of fluctuations that it can physically resolve. The high-frequency temporal response is a measure of how quickly the instrument can respond to a change in the fluctuating field. The response transfer function, which corrects for some of the shortcomings, is available for some sensors (Soulsby 1980; Ninnis 1984).

Shear probes cannot resolve fluctuations whose wavelengths are comparable to the diameter of the probe. Ninnis (1984) has computed a transfer function which compensates for this spatial averaging, for wavelengths longer than $\approx$0.6 cm. We use his transfer function to boost our spectra slightly at short wavelengths (high wavenumbers). However, no corrections can be computed for wavelengths less than 0.6 cm. We consider the calculation of $\epsilon$ to be acceptable if 75% of the dissipation spectrum is at wavelengths longer than 0.606 cm ($k > 1040$ m$^{-1}$). When $\epsilon$ is computed from $\partial u/\partial z$, 75% of the dissipation is at wavelengths less than $0.38k_s$ (Dewey 1987). Since all our measurements are from more than 0.15 m above the bottom, and $\epsilon = \rho u_*^3/\kappa z$, this criterion is met if $u_* < 2.2$ cm s$^{-1}$. All friction velocities observed on the continental shelf were well below this level.

5) *Isotropy:* As noted previously, turbulence can be considered isotropic at wavelengths less than the distance to the bottom ($\lambda < z$), or at wavenumbers greater than $2\pi/z$ (Pond 1965). We consider an acceptable limit to be one where fluctuations measured at 0.15 m from the bottom are both isotropic and at the peak of the dissipation spectrum. Denoting this wavelength as $\lambda_p$, for the peak of the spectrum, the criterion is $z > \lambda_p$, and for radian wavenumbers it is $z > 2\pi/k_p$. The peak of the universal $G_2(k/k_s)$ spectrum is at $k_p = 0.13k_s$. Upon substitution of $k_s = (\epsilon\rho^2/\mu^3)^{1/4}$, $\epsilon = \rho u_*^3/\kappa z$ and $\lambda = 2\pi/k$, the criterion becomes

$$z > 1.9 \times 10^{-4} u_*^{-1}, \tag{14}$$

where $z$ is in meters and $u_*$ in m s$^{-1}$. The minimum $u_*$ which meets this criterion at $z = 0.15$ m is $u_* = 0.0013$ m s$^{-1}$, a small value on the shelf. The observations presented here represent data collected above $z = 0.15$ m, therefore, we may consider the above criterion to be very conservative.

6) The uncertainties associated with sensor calibrations and with using (10) to calculate the microstructure shear $\partial u/\partial z$ will now be addressed. The fall speed $W$ changes very slowly with depth and is calculated at each depth from the differentiated fourth order fit to the pressure record. Our maximum error of 5% in $W$ results in a 10% error in $\partial u/\partial z$ and a 20% error in $\overline{\partial u/\partial z)^2}$. The differentiator gain $G$ is known to approximately 2%. The shear probe calibration $S$ is known to approximately 7%, which reflects the standard deviation in the constants obtained from multiple calibrations over time. The cumulative error estimated in the shear $\partial u/\partial z$ is then 19%, which translates to an approximate uncertainty in the variance $\overline{(\partial u/\partial z)^2}$ of 38%. The dynamic viscosity $\mu$ is predominantly temperature dependent and is calculated assuming a mean salinity of 32.5‰ from the formula of Miyake and Koizumi (1948). An estimated uncertainty of 5% in $\mu$ adds to give a total uncertainty in $\epsilon$ of 43%. This is a conservative estimate for the uncertainty, in that all the errors have been added linearly. Most of these contributions are random, and a more realistic estimate of the uncertainty is obtained by adding the square root of the individual uncertainties. This approach leads to an uncertainty in $\epsilon$ of approximately 20%. This assumes that the full variance can be recovered by the integration of $k_3{}^2\phi_{11}(k_3)$ from $k_l$ to $k_u$ (11). Dewey (1987) estimates that when the signal-to-noise ratio is maximized, the true variance can be recovered to within 10%. The estimated uncertainty for individual $\epsilon$ estimates in the constant stress layer is then $\sim$30%.

We can now address the errors introduced in the calculation of $u_*$ using (6). The density $\rho$ is known to at least 1% and is calculated from the local temperature

and conductivity as measured by the FLY II profiler. The distance to the bottom $z$ is known to within 5%. The error due to nonstationarity in the time series was previously estimated to be ≤3%. The cumulative uncertainty in $u_*$ from a single $\epsilon$ value in the constant stress layer is then about 16%.

## 6. Bottom stress estimates

Figure 2 shows a dissipation rate profile (No. 506) from station M2. The bottom stress has been found by taking the individual dissipation rate values within the constant stress layer $\epsilon_i$, evaluating $u_{*i}$ using (6) for each, and averaging these to give a single estimate of the bottom stress for this profile,

$$\tau_0 = \bar{\rho}\,\frac{\sum_{i=1}^{i=N_{CSL}} u_{*i}^2}{N_{CSL}}, \qquad (15)$$

where $N_{CSL}$ is the number of dissipation rate values that are in the constant stress layer (CSL).

The height of the CSL is theoretically arbitrary and depends on the choice of a threshold, say $\gamma$, at which point the Reynolds stress deviates from the bottom stress, $|\tau - \tau_0| \approx \gamma$. Determining the height of the CSL is therefore subjective, and we have selected a height at which there is a local minimum in the standard deviation of the running average $\overline{u_*}|_{i-3}^{i}$, calculated over the preceding four $u_{*i}$ values. (This running average is given by $\overline{u_*}|_{i-3}^{i} = \sum_{i-3}^{i} u_{*i}/4.$) This technique identifies the height at which the $u_{*i}$ values calculated using (6) start to deviate from the nearly constant values immediately next to the bottom. This process biases the CSL thickness since the minimum thickness is ~0.8 m, the height that includes the first four $u_{*i}$ values. This bias however does not seem to introduce overestimates, as the height identified is always very near the height that would be selected had the CSL thickness been determined manually (by eye) from the dissipation rate profile. Table 1 shows the $u_{*i}$ estimates from the near-bottom $\epsilon_i$ values and the identified CSL height for the dissipation rate profile shown in Fig. 2. The uncertainty indicated for $\overline{u_*}$ is the standard deviation from the $N_{CSL}u_{*i}$ estimates, and does not include the experimental uncertainty estimated in the preceding section.

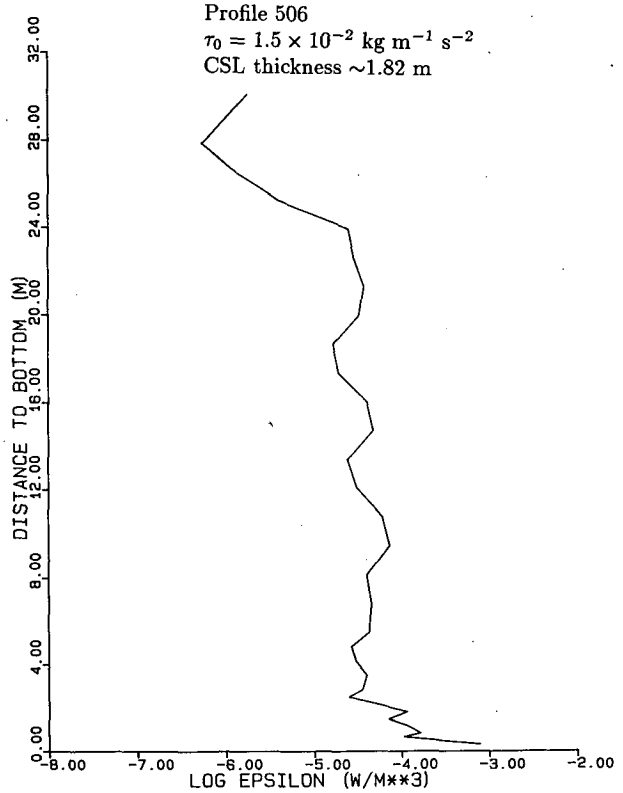


FIG. 2. Log dissipation rate values calculated from microstructure shear profile 506 at M2. The bottom stress has been estimated from the dissipation rates within the constant stress layer, estimated to be ~1.8 m thick. The uncertainty indicated in $\tau_0$ represents the standard deviation in the seven individual estimates of $u_*$ from the seven $\epsilon$ values in the constant stress layer. The data were collected at M2, 17 June 1985.

TABLE 1. Table of individual $\epsilon$ and $u_*$ values and estimated CSL height for profile 506 at M2.

| $z_i$ (m) | $\epsilon_i$ W m$^{-3}$ × 10$^{-4}$ | $u_{*i}$ (cm s$^{-1}$) | $\overline{u_*}\|_{i-3}^{i}$ (cm s$^{-1}$) | Standard deviation in $\overline{u_*}\|_{i-3}^{i}$ | $\overline{u_*}\|_{1}^{i}$ (cm s$^{-1}$) |
|---|---|---|---|---|---|
| 0.32 | 7.765 | 0.463 | | | |
| 0.49 | 2.631 | 0.372 | | | |
| 0.65 | 1.056 | 0.301 | | | |
| 0.82 | 1.638 | 0.377 | 0.378 | 17.5% | 0.378 |
| 1.15 | 1.181 | 0.379 | 0.357 | 10.4% | 0.378 |
| 1.49 | 0.703 | 0.347 | 0.351 | 10.3% | 0.373 |
| 1.82 | 0.115 | 0.437 | 0.385 | 9.7%⇐ | 0.382 |
| 2.16 | 0.543 | 0.361 | 0.381 | 10.4% | 0.380 |
| 2.49 | 0.246 | 0.291 | 0.359 | 16.8% | 0.370 |
| 2.82 | 0.354 | 0.342 | 0.357 | 16.9% | 0.367 |

⇒ $\overline{u_*} \approx 0.382$ cm s$^{-1}$ ± 14.1%
CSL height ≈ 1.82 m

Figure 3 shows the same profile in Fig. 2 but with a logarithmic ordinate. The dashed line represents the theoretical dissipation rates as calculated using (6) and the friction velocity obtained from the measured dissipations (Table 1). The cubic relation between $\epsilon$ and $u_*$ fixes the slope of the theoretical $\epsilon$ profile in a log–log plot (dashed line in Fig. 3). The gradual departure of the measured $\epsilon$ profile from the CSL distribution (6) implies that there is no abrupt transition in the stress at the top of the CSL and that the Reynolds stress $\tau$ deviates slowly from the constant stress value $\tau_0$. The CSL height estimates vary from profile to profile due to the intermittency of the turbulence. The technique outlined above consistently identifies the CSL height

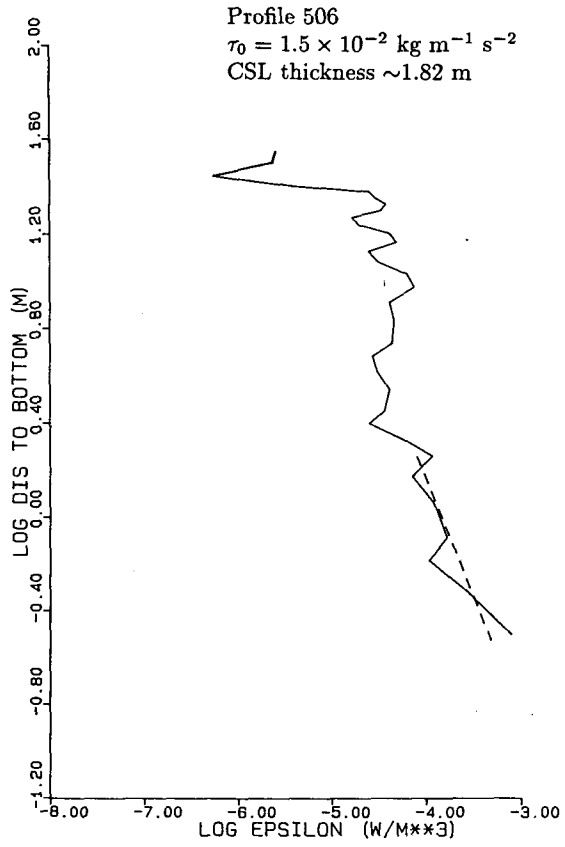


FIG. 3. Same data shown in Fig. 2, but with a log ordinate. The dashed line is the distribution of $\epsilon$ found by fitting the calculated value of $u_*$ to (6).

that is apparent to the eye from plots such as Fig. 3. Confidence in both $u_*$ and the CSL height can be improved by averaging several dissipation rate profiles.

Ensemble average dissipation rates are obtained by averaging the dissipation rates at fixed heights from consecutive profiles. The dissipation is averaged over all profiles, then the constant stress relationship is fitted. The standard deviation in $\overline{u_*}$ calculated from the average $\bar{\epsilon}$ values is typically 10% for a series of profiles. The lognormal variance is typically $\sigma^2_{\ln u_*} = 0.11$. Figure 4 shows the average dissipation rates from a series of three quasi-synoptic profiles, and the associated friction velocity and CSL height.

The CSL is resolved with more confidence when many profiles can be averaged. Turbulent dissipation rate profiles from station W05 in Hecate Strait were collected in July 1983 in water 35 m deep. Series of 20 profiles were obtained over periods of approximately 40 minutes. For these measurements the profiler carried two orthogonally aligned shear probes so that two dissipation rate profiles could be calculated for each profiler descent. Therefore, 40 individual dissipation rate profiles were collected in ~40 minutes. Figure 5 shows an average of 20 individual profiles obtained in 18 minutes. Standard deviations in the friction velocities calculated from these average dissipation rates are consistently less than 10%, and have been as low as 3%. Lognormal variances are similarly lower, with typical values of $\sigma^2_{\ln u_*} = 0.1$, and the lowest recorded being $\sigma^2_{\ln u_*} = 0.05$.

## 7. Discussion

The dissipation rate measurements made in 1985 on the continental shelf west of Vancouver Island were collected over a complete diurnal tidal cycle. Time series of one-hour average friction velocities and the average current magnitude $\overline{U(3)}$ at 3 meters above the bottom are shown in Fig. 6. The current mooring was approximately 1 km north of the microstructure observations; therefore local fluctuations in the current data over short periods (10 minutes) may not represent flow fluctuations at the microstructure site, and visa versa. The values $\overline{u_*}$ and $\overline{U(3)}$ in Fig. 6 are therefore one-hour averages. In this case, the $\overline{u_*}$ values are the averages of the ten individual estimates of $u_*$ from ten profiles. The correlation coefficient between the friction velocity and current magnitude at $z = 3$ m is $R^2 = 0.94$, at zero phase lag. A similar comparison was not possible

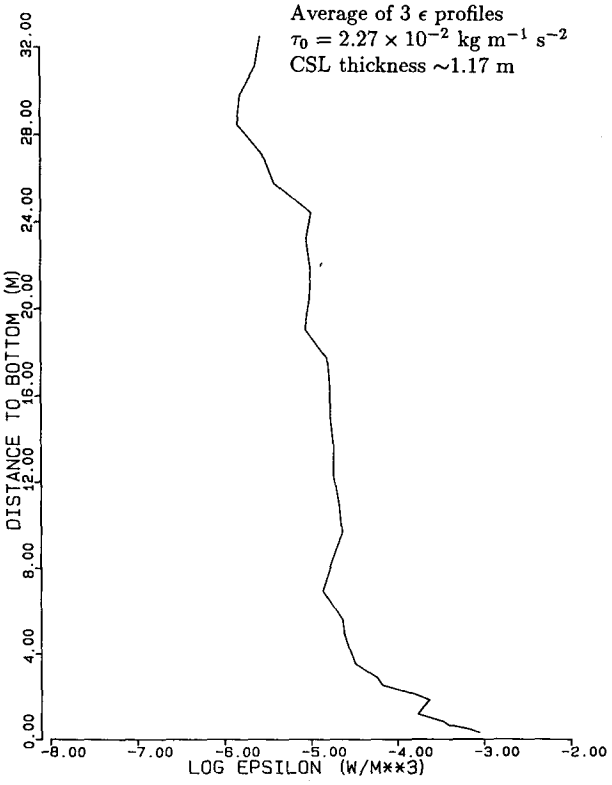


FIG. 4. Average dissipation rate values obtained by averaging three consecutive profiles, obtained in 9 minutes. The averaging reduces the effect of intermittency and improves the resolution of the constant stress layer and the uncertainty in the bottom stress estimate.

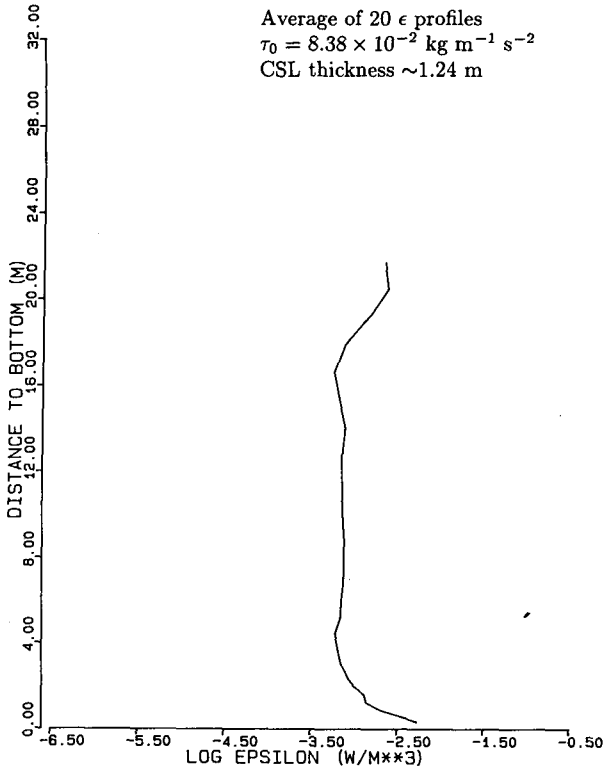


FIG. 5. Average dissipation rate values obtained by averaging 20 individual dissipation rate profiles collected in 18 minutes. The data are from Hecate Strait, station W05, July 1983. Total water depth is 35 m.

for the Hecate Strait data due to a malfunction in the current meter placed near the bottom.

A drag coefficient can be estimated from the friction velocity and current magnitude time series. The drag coefficient at one meter $C_D$ is defined here as

$$C_D = \frac{\overline{u_*^2}}{\overline{U(1)^2}}. \tag{16}$$

The current at one meter above the bottom is extrapolated from a least-squares fit of the measured values of $\overline{u_*}$ and $\bar{U}(3)$ to (3). The average drag coefficient at M2 is found to be

$$C_D = 0.69 \times 10^{-3} \ (\pm 22\%),$$

where the uncertainty is the standard deviation from 11 individual $C_D$ estimates.

This $C_D$ value suggests that the flow is hydrodynamically smooth (Sternberg 1968). A viscous sublayer then underlies the constant stress layer. From (3) the height of the viscous sublayer, $\delta$, is found to vary between 0.7 and 4.6 cm over a diurnal cycle, in good agreement with the measurements of Caldwell and Chriss (1979). Over the diurnal period the height of the viscous sublayer is found to be proportional to the viscous length scale ($\nu/u_*$), represented as

$$\delta \approx (28.8 \pm 5.9) \frac{\nu}{u_*},$$

as required by the concept of universal similarity. The constant 28.8 is twice that found from laboratory experiments (Monin and Yaglom 1975, p. 277), but close to some of the values ($\sim$20) measured on the Oregon shelf by Chriss and Caldwell (1984). The latter believe that the constant is not universal.

A bottom grab at M2 revealed that the sediments were made up of a sticky mud, a surface that is very likely to be "smooth". No information about bed forms and local topographic irregularities was available and an estimate of the actual bottom "roughness" is not possible.

Chriss and Caldwell (1982) indicate that under hydrodynamically smooth conditions the actual bottom stress can be as much as four times lower than the stress calculated from current measurements in the logarithmic portion ($z > 1$ m) of the boundary layer. When the stress is calculated from the slope of (3) fitted to the current measurements made at 3, 5 and 10 m above the bottom, the values obtained are consistently 4.5 times larger than the estimates found from the dissipation rate profiles. In predicting a higher bottom stress (higher $u_*$), the method of fitting a logarithmic function to current measurements in this region also predicts a rougher bottom (smaller $\delta$) and a higher drag coefficient ($3.1 \times 10^{-3}$).

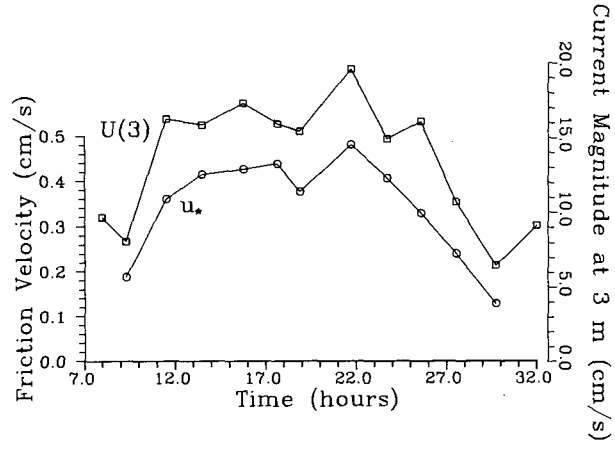


FIG. 6. Time series of average friction velocities and the average current magnitude from station M2 and mooring C2, respectively. The microstructure observation period spans 21 hours, almost one complete diurnal cycle. The squared correlation coefficient between these series is $R^2 \approx 0.94$ and the associated drag coefficient is $C_D = 0.69 \times 10^{-3}$. The observations were made between 0900 PST 17 June and 0600 PST 18 June 1985. Time is shown from the start of 17 June. The water depth was approximately 135 m.

The discrepancy between the bottom stress estimates calculated from dissipation rate profiles and those from the current velocity data has two significant consequences. First, the current data is outside the estimated constant stress layer and although the current profile may be approximated by a logarithmic function (average correlation coefficient of $R^2 \approx 0.87$), the extrapolation that gives the bottom stress from that function is inaccurate. Second, the influence of form drag on the current meter measurements (Chriss and Caldwell 1982), is important when irregularities in the boundary surface influence the total stress farther from the boundary, outside the constant stress layer. No information on the nature of any bed-forms is available and an estimate of the form drag is therefore impossible.

Skin friction dominates the Reynolds stress within the constant stress layer and determines the sediment transport conditions. Therefore, the dissipation rate measurements down to 0.15 m above the bottom are more valuable for estimating both stress and sediment transport than are current measurements made above the CSL. These discrepancies indicate the importance of pressure fluctuations (form drag) on the current as measured by conventional current meters. This indication is only possible when both turbulent (microstructure) and mean (current) quantities are measured simultaneously.

*Acknowledgments.* The authors would like to thank K. Lee, G. Chase and C. McKay for technical support, Drs P. H. LeBlond and A. Gargett for support and advice, Captain Ray MacKenzie, officers and crew of the CCS *Vector* for deployment, and the reviewers for helpful comments. Funding was partly provided to RKD by a grant from the Science Subvention Fund of the Department of Fisheries and Oceans.

## REFERENCES

Baker, M. A., and C. H. Gibson, 1987: Sampling turbulence in the stratified ocean: Statistical consequences of strong intermittency. *J. Phys. Oceanogr.*, **17**(10), 1817–1836.

Caldwell, D. R., and T. M. Chriss, 1979: The viscous sublayer at the sea floor. *Nature*, **205**, 1131–1132.

Chriss, T. M., and D. R. Caldwell, 1982: Evidence for the influence of form drag on bottom boundary layer flow. *J. Geophys. Res.*, **87**, 4148–4154.

——, and ——, 1984: Universal similarity and the thickness of the viscous sublayer at the ocean floor. *J. Geophys. Res.*, **89**, 6403–6414.

Crawford, W. R., 1984: Energy flux and generation of shelf waves along Vancouver Island. *J. Phys. Oceanogr.*, **14**, 1599–1607.

——, and T. R. Osborn, 1979: Microstructure measurements in the Atlantic equatorial undercurrent during GATE. *Deep-Sea Res.* (GATE Suppl. II), **26**, 285–308.

——, and R. E. Thomson, 1984: Diurnal-period continental shelf waves along Vancouver Island: A comparison of observations with theoretical models. *J. Phys. Oceanogr.*, **14**, 1629–1646.

Dewey, R. K., 1987: Turbulent energy dissipation over the continental shelf., Ph.D. thesis, University of British Columbia, Canada, 205 pp.

——, W. R. Crawford, A. E. Gargett and N. S. Oakey, 1987: A microstructure instrument for profiling oceanic turbulence in coastal bottom boundary layers. *J. Atmos. Oceanic Technol.*, **4**(2), 288–297.

Gargett, A. E., T. R. Osborn and P. W. Nasmyth, 1984: Local isotropy and the decay of turbulence in a stratified fluid. *J. Fluid Mech.*, **144**, 231–280.

Grant, W. D., and O. S. Madsen, 1979: Combined wave and current interaction with a rough bottom. *J. Geophys. Res.*, **84**, 1797–1808.

——, and ——, 1986: The continental-shelf bottom boundary layer. *Ann. Rev. Fluid Mech.*, **18**, 265–305.

——, A. J. Williams III and S. M. Glenn, 1984: Bottom stress estimates and their prediction on the northern California continental shelf during CODE-1: The importance of wave–current interaction. *J. Phys. Oceanogr.*, **14**, 506–527.

Gross, T. F., and A. R. M. Nowell, 1985: Spectral scaling in a tidal boundary layer. *J. Phys. Oceanogr.*, **15**, 496–508.

Gust, G., 1985: Comments on "Bottom stress estimates and their prediction on the northern California continental shelf during CODE-1: The importance of wave-current interaction". *J. Phys. Oceanogr.*, **15**, 1229–1237.

Hinze, J. O., 1975: *Turbulence.*, 2nd ed., McGraw-Hill series in Mech. Eng., McGraw-Hill, 618 pp.

Huntley, D. A., 1985: Comments on "Bottom stress estimates and their predictions on the northern California continental shelf during CODE-1: The importance of wave-current interaction." *J. Phys. Oceanogr.*, **15**, 1217–1218.

——, 1988: A modified inertial dissipation method for estimating sea bed stresses at low Reynolds numbers, with application to wave–current boundary layer measurements. *J. Phys. Oceanogr.*, **18**, 339–346.

——, and D. G. Hazen, 1988: Sea bed stresses in combined wave and steady flow conditions on the Nova Scotia continental shelf: Field measurements and predictions. *J. Phys. Oceanogr.*, **18**, 347–362.

Kolmogoroff, A. N., 1941: The local structure of turbulence in an incompressible viscous fluid for very high Reynolds number. *C.R. Acad. Sci. USSR*, **30**, 301–305.

Miyake, Y., and M. Koizumi, 1948: The measurement of the viscosity coefficient of sea water. *J. Mar. Res.*, **7**, 63–66.

Monin, A. S., and A. M. Yaglom, 1975: *Statistical Fluid Mechanics: Mechanics of Turbulence, Vol. 2.* The MIT Press, 874 pp.

Ninnis, R., 1984: The spatial transfer function of the airfoil turbulence probe. Ph.D. thesis, University of British Columbia, 94 pp.

Oakey, N. S., and J. A. Elliott, 1982: Dissipation within the surface mixed layer. *J. Phys. Oceanogr.*, **12**, 171–185.

Osborn, T. R., 1974: Vertical profiling of velocity microstructure. *J. Phys. Oceanogr.*, **4**, 109–115.

——, and W. R. Crawford, 1980: An airfoil probe for measuring turbulent velocity fluctuations in water. *Air–Sea Interactions: Instruments and Methods.*, F. Dobson, L. Hasse and R. Davies, Eds., Plenum, 801 pp.

Pond, S., 1965: Turbulence spectra in the atmospheric boundary layer over the sea. Ph.D. thesis, University of British Columbia, Vancouver, B.C., 175 pp.

Press, W. H., B. P. Flannery, S. A. Teukolsky and W. T. Vettering, 1986: *Numerical Recipes.* Cambridge University Press, 818 pp.

Richards, K. J., 1982: Modeling the benthic boundary layer. *J. Phys. Oceanogr.*, **12**, 428–439.

Scorer, R. S., 1985: A vivid mechanical picture of turbulence., *Turbulence and Diffusion in Stable Environments*, J. C. R. Hunt Ed., Oxford University Press, 97–109.

Soulsby, R. L., 1980: Selecting record length and digitization rate for near-bed turbulence measurements. *J. Phys. Oceanogr.*, **10**(2), 208–219.

——, 1983: The bottom boundary layer of shelf seas. *Physical Oceanography of Coastal and Shelf Seas*, B. John Ed., Elsevier Oceanogr. Ser. **35**, 189–266.

Sternberg, R. W., 1968: Friction factors in tidal channels with differing bed roughness. *Mar. Geol.*, **6**, 243–260.